Published in final edited form as:

Lab Chip. 2020 March 03; 20(5): 987–994. doi:10.1039/c9lc01124b.

Acoustic tweezers based on circular, slanted-finger interdigital transducers for dynamic manipulation of micro-objects†

Putong Kang[‡,a], **Zhenhua Tian**[‡,b], **Shujie Yang**[‡,a], **Wenzhuo Yu**[a], **Haodong Zhu**[a], **Hunter Bachman**[a], **Shuaiguo Zhao**[a], **Peiran Zhang**[a], **Zeyu Wang**[a], **Ruoyu Zhong**[a], **Tony Jun Huang**[a]

[a]Department of Mechanical Engineering and Materials Science, Duke University, Durham, NC 27708, USA

[b]Department of Aerospace Engineering, Mississippi State University, Starkville, MS 39762, USA

Abstract

Acoustic tweezing technologies are gaining significant attention from the scientific communities due to their versatility and biocompatibility. This study presents acoustic tweezers based on circular, slanted-finger interdigital transducers (CSFITs), which can steer the propagation direction of surface acoustic waves (SAWs) by tuning the excitation frequency. The CSFITs based acoustic tweezers enable dynamic and reconfigurable manipulation of micro-objects using multi-tone excitation signals. Compared to traditional interdigital transducers that generate and control SAWs along one axis, the CSFITs allow for simultaneously generating and independently controlling SAWs propagating along multiple axes by changing the frequency composition and the phase information in a multi-tone excitation signal. Moreover, the CSFITs based acoustic tweezers can be used for patterning cells/particles in various distributions and translating them along complex paths. We believe that our design is valuable for cellular-scale biological applications, in which on-chip, contactless, biocompatible handling of bioparticles is needed.

Introduction

Researchers in biology, chemistry, engineering, physics, and medicine need biocompatible, precise manipulation methods[1] to deal with cellular-scale samples,[2,3] such as microparticles,[4] cells,[5–7] and organisms.[8] Various solutions for these manipulation needs have been developed, including optical,[9,10] electrokinetic,[11] magnetic,[12,13] and acoustic based methods.[14–22] In particular, acoustic-based manipulation methods, such as surface acoustic wave (SAW)-based acoustic tweezers, have advantages in terms of versatility, precision, and biocompatibility. In fact, acoustic-based techniques have been demonstrated for realizing

†Electronic supplementary information (ESI) available. See DOI: 10.1039/c9lc01124b

tony.huang@duke.edu.

Author contributions

P. K., Z. T., and S. Y. planned and designed the research; P. K., Z. T., and P. Z. did the simulation; P. K., W. Y., H. Z. and S. Z. performed experiments; P. K. and H. Z. fabricated the device; Z. W. and R. Z. prepared the cells. Z. T., S. Y., P. K. and T. J. H. conceived the idea; P. K., Z. T. and H. B. wrote the draft, and all authors contributed to editing the manuscript.

‡These authors contributed equally to this work.

Conflicts of interest

There are no conflicts to declare.

several critical functionalities, such as particle/cell manipulation,[15,23–26] tomography of bio-particles,[27] cell printing,[28] particle/cell separation,[29–31] cell analysis,[32,33] cell sorting,[34,35] reagent mixing and pumping,[36,37] diagnostics,[38,39] and particle/cell patterning.[40–43]

To enable the functions mentioned above, researchers must precisely design and optimize the device's interdigital transducers (IDTs). The SAW-based acoustic tweezer devices typically rely on one or more pairs of IDTs deposited onto a piezoelectric substrate to generate the desired SAW pressure fields for manipulations;[44] the electrode configuration of the IDTs significantly affects SAW field generation, which determines the functionality of the tweezers. As a result, researchers have developed multiple types of IDTs with different electrode configurations to realize their desired functionalities for lab-on-a-chip applications. For example, three types of single-phase unidirectional transducers (SPUDTs), including straight SPUDTs, concentric circular, and elliptical SPUDTs, were designed for concentration/separation of microparticles.[45] Both the circular and elliptical SPUDTs provided enhanced ability to focus SAWs and improve fluid actuation as well as the manipulation of particles at microscale dimensions. However, even though these designs provided some flexibility, it remained difficult to achieve dynamic manipulation of micro-objects using these transducers. In order to achieve dynamic manipulation, Antoine Riaud *et al.* introduced a circular array of IDTs capable of synthesizing classical wave fields; still, high-end programmable multichannel electronics with high costs were required to drive and control multiple IDTs at these high frequencies.[46,47] On the other hand, researchers developed slanted-finger interdigital transducers (SFITs) with chirped electrode configurations to achieve dynamic acoustic manipulations. By tuning the frequency delivered to the SFIT-based acoustic tweezers, the interspacing of grid-like acoustic pressure field patterns can be dynamically changed.[48,49] However, since the SFITs can only generate SAWs along one axis, they are only capable of generating simple SAW fields, having limited controllability and degrees of freedom. For example, changing the direction of the SAWs or rotating a pattern of particles cannot be realized with those SFIT-based acoustic tweezers; this is a critical drawback, because rotational manipulation is important for developing on-chip tomography techniques for characterizing cells[7,27] and microorganisms.[50]

In this study, we present circular, slanted-finger interdigital transducers (CSFITs) that are able to steer the propagation direction of SAWs by changing the excitation frequency and simultaneously generating/controlling SAWs in multiple directions by using a multi-tone input signal. We show that our CSFIT-based acoustic tweezers can enable dynamic and reconfigurable manipulation of micro-objects using multi-tone excitation signals. The developed CSFITs have angularly varying finger widths and spacings. Such variations along the angular direction introduce a new degree of freedom, *i.e.*, tuning of the SAW direction. When the excitation frequency of the input signal for a CSFIT changes, different angular sections of the CSFIT respond to the excitation frequency. Therefore, the SAW direction and wavelength can be controlled by the frequency input. Another new feature enabled by the CSFIT is frequency-domain multiplexing; the CSFIT allows for simultaneous generation of SAWs that propagate in multiple directions, as well as independent control of those SAWs using a multi-tone radio frequency excitation signal. By taking advantage of the new features enabled by CSFITs, the new CSFIT-based acoustic tweezers can generate various potential well patterns for dynamic and reconfigurable particle or cell manipulation. By encoding

desired frequency and phase information into a multi-tone excitation signal, we experimentally demonstrate a range of functions of our acoustic tweezers, including 1D patterning of cells, dynamic reconfiguration of 2D patterns of microparticles, and translation of a single microparticle along desired paths.

Methods

Working mechanism

The CSFIT-based, frequency-multiplexed acoustic tweezers are composed of a pair of CSFITs that are in a centrosymmetric distribution with respect to the coordinate origin O, as shown in Fig. 1a. A photo of the fabricated CSFIT-based acoustic tweezers chip with a disposable microfluidic chamber is shown in Fig. 1b. For our CSFIT-based acoustic tweezers design, each CSFIT is composed of 27 pairs of electrodes distributed along the radial direction. The widths of the electrodes and finger spacings gradually change with respect to the angular direction. Assuming that several radial lines divide the CSFIT into angular sections, each angular section can be considered as a small, 'traditional' IDT with straight electrodes. Considering that the finger spacing varies along the angular direction, infinitesimal sections of the CSFIT oriented in different directions should respond to different excitation frequencies. The relation between excitation frequency f_θ and finger spacing d_θ is $f_\theta = c_\theta/4d_\theta$, where c_θ is the phase velocity of SAWs in the θ direction. The wavenumber of generated SAW in the θ direction is $k_\theta = \pi/2d_\theta$. From the relationship between the frequency and the electrode configuration, it is found that different angular sections of the CSFIT can respond to different input frequencies; thus, we can activate different sections of the CSFIT by utilizing varied input frequencies. In other words, the propagation direction and wavelength of generated SAWs can be tuned by changing the excitation frequency.

The CSFIT also introduces a frequency-multiplexing capability as illustrated in Fig. 1c. When an excitation signal composed of multiple frequency components is transmitted into the CSFIT, angular sections with resonant frequencies that match the excitation frequency components will simultaneously generate traveling SAWs in multiple directions. The input for the CSFIT is a multi-tone excitation signal composed of M distinct frequency components denoted as $[f_{\theta_m}]_M$. The phases and amplitudes of those frequencies are denoted as $[\varphi_{\theta_m}]_M$ and $[A_{\theta_m}]_M$. As shown in Fig. 1c, when a multi-tone signal is used, the CSFIT can decompose the input multi-tone signal based on the frequency-filtering function $G_{\theta_m}(f, k)$ of each angular section; the frequency-filtering function is a relationship between the resonance frequencies and geometric properties of the system. In this example, three angular sections in the directions of θ_1, θ_2, and θ_3 respond to the excitation signal, and as a result, three SAWs traveling in those different directions are generated. Each SAW contains only one frequency component f_{θ_m} with the corresponding phase φ_{θ_m} and amplitude A_{θ_m}.

When two CSFITs in a centrosymmetric arrangement are excited at a frequency f_θ, the interference of traveling SAWs generated by the two CSFITs forms standing SAWs (SSAWs) along the θ direction. As shown in Fig. S1,† we name the section in the θ direction

†Electronic supplementary information (ESI) available. See DOI: 10.1039/c9lc01124b

IDT_{θ}^{R} and its couple in the $\theta + \pi$ direction IDT_{θ}^{L}. These two sections are denoted as the θth pair. The two sections in a pair have the same finger spacing, so they have the same resonance frequency f_{θ}. With counter-propagating traveling SAWs generated by the paired angular sections, the interference will create SSAWs with pressure node lines perpendicular to the direction of θ. These pressure node lines can be used for the manipulation of micro-objects. Detailed configurations of the CSFIT-based acoustic tweezers are given in ESI.†

When the excitation signal has two frequency components f_{θ_1} and f_{θ_2}, two pairs of angular sections in the CSFIT-based acoustic tweezers generate SAWs to form 2D potential well distributions, as shown in Fig. S2.† Moreover, these two pairs can be independently controlled based on the frequency-multiplexing feature of our acoustic tweezers. Therefore, when the excitation signal has two frequency components, the CSFIT-based acoustic tweezers can be used for patterning micro-objects in 2D grid-like distributions and for dynamically manipulating the 2D distributions. Compared to previous acoustic tweezers, our design takes advantage of the CSFIT's frequency multiplexing capability and achieves filtering of continuous multi-tone excitation signals. Without using complex and expensive equipment, such as multichannel function generators, high-speed multiplexers, and multiple amplifiers, our acoustic tweezers can generate and reconfigure 2D patterns by modulating phases/amplitudes at selected frequencies or by changing the combination of frequencies used in the excitation signal.

Device design and fabrication

Here, we describe a general design rule for the CSFIT based acoustic tweezers. To realize a tunable SAW frequency ranging from f_{min} to f_{max} on a piezoelectric wafer, the desired finger spacings for the CSFIT can be calculated using the previously defined frequency–spacing relationship equation. By gradually varying the finger spacings with respect to the angular direction, the resonance frequency will be changed per the defining equation, which dictates the variable frequency CSFIT design. For the CSFIT-based acoustic tweezers, two CSFITs are arranged in a centrosymmetric configuration with respect to the center of the acoustic tweezers.

In this study, the *X*-cut $LiNbO_3$ substrate is selected for designing the CSFITs, since it allows for efficiently generating SAWs in a wide range of directions and it has a low beamforming effect induced by the inherent anisotropic piezoelectric material properties. In contrast, the commonly used 128° *Y*-cut $LiNbO_3$ is not suitable for designing CSFITs, because it has strong inherent beamforming effect and a relatively small range of useful directions for efficiently generating SAWs.

Besides the cut of the $LiNbO_3$ crystal, the direction-dependent electromechanical coupling coefficients introduced by the anisotropic material properties of the piezoelectric substrate should be considered. For directions with low coupling coefficients, it is inefficient to generate SAWs by using IDTs. Therefore, in the design of CSFITs, we set the bus bar electrodes of the CSFITs in the directions with low coupling coefficients and avoided using these directions for generating SAWs and designing acoustic tweezers.

To fabricate the CSFITs, electrodes were deposited onto a 0.5 mm thick *X*-cut $LiNbO_3$ substrate using standard microfabrication processes including photolithography, e-beam evaporation, and lift-off processes. The phase velocities of SAWs in the substrate are given in Fig. 2a. To fabricate the electrodes of the CSFITs, the $LiNbO_3$ wafer was coated with a layer of SPR3012 photoresist (MicroChem, USA), followed by optical lithography and chemical development. Then, chrome and gold layers (Cr/Au) were deposited onto the $LiNbO_3$ substrate by evaporation, followed by a lift-off process to form a pair of CSFITs. Each CSFIT has 27 pairs of electrodes to fully develop the SAWs.

The microfluidic chamber for hosting fluids and micro-objects is disposable; that is, the chamber can be peeled off of the $LiNbO_3$ substrate and replaced by a clean chamber after experimentation. The chamber was composed of two polydimethylsiloxane (PDMS) layers, including a top layer with a microfluidic chamber (around 50 μm in height), and a thin bottom layer (around 30 μm thick) to seal the chamber. The top layer was fabricated by photolithography and PDMS replica molding. First, silane vapor (Chlorotrimethylsilane, Sigma Aldrich, USA) modified the surface of the mold for 20 minutes. Then, a mixture of PDMS base and cross-linker (Sylgard 184, Dow Corning, USA) at a ratio of 7: 1 (w/w) was poured onto the mold and then cured at 65 °C for an hour to form an open microfluidic chamber. Then, a puncher was used to form an inlet and outlet at designated positions. At the same time, a silicon wafer was prepared with a spin-coated PDMS layer (30 μm thick for the bottom layer). After baking both PDMS components at 65 °C for 20 minutes, the prepared top layer bonded with the bottom layer. After further baking them at the same temperature for an hour, the open chamber (top PDMS layer) was fully sealed by the bottom PDMS layer to form a closed microfluidic chamber with an inlet and an outlet. The PDMS was peeled off of the silicon wafer, and the combined chips were each cut to an ideal size for further use.

Experimental setup

The experiments were conducted on the stage of an inverted microscope (Nikon TE2000U). The excitation signals were generated by a function generator (AFG3011, Tektronix), amplified to 10 Vpp through a power amplifier (25A250A, Amplifier Research). The signal generator was controlled by a MATLAB program which precisely modulated the frequency, phase, and amplitude of the excitation signal. Images and videos were taken using Nikon imaging software (NIS-Advanced, Nikon) through a CCD digital camera (CoolSNAP HQ2, Photometrics).

Microparticle and cell sample preparation

10.2 μm yellow-green polystyrene (PS) microspheres (Magsphere Inc.) were mixed in deionized (DI) water to an approximate concentration of 1×10^6 mL^{-1}. K562 cells (American Type Culture Collection (ATCC®) CCL-243™) were cultured in RPMI 1640 (Gibco, Life Technologies) medium containing 1% penicillin/streptomycin (PIS) and 10% fetal bovine serum (FBS). The K562 cells were maintained in 5% CO_2, 37 °C cell culture incubators (HERAcell VIOS 160i CO_2 Incubator, Thermo Fisher Scientific). Since K562 cells were non-adherent cells and would not clump, there was no need to use Trypsin to resuspend cells. Before each experiment, the RPMI 1640 medium was replaced, and cells

were diluted to an approximate concentration of 1×10^7 mL^{-1}. The suspension was injected into the chamber using a 1 mL syringe (309659, Becton Dickinson).

Cell viability assays

Cell viability assays were performed on cells in different groups: a control group without any SAWs and three test groups with different exposure durations (3, 15, and 45 min) of SAWs generated with an 8 Vpp excitation signal. For each group, the dead cell staining was performed using trypan blue (Gibco) right after exposure. The cell viability was obtained by counting the number of blue stained cells compared to the total number of cells. Cells were counted as dead if they took up the trypan blue.

3D model for finite element simulations

To investigate the SAW generation mechanism of the CSFIT based acoustic tweezers, numerical simulations were conducted with the finite element software COMSOL Multiphysics®. A 3D model for the simulation is given in Fig. 2b. The finite element model is composed of a 0.5 mm thick *X*-cut $LiNbO_3$ substrate simulated by the piezoelectric module. The material properties of the $LiNbO_3$ substrate are given in section S2.† The model is based on a simplified configuration of a CSFIT, which has only 9 pairs of electrode fingers. The simplified configuration improved the computation speed of the 3D simulation. Since the directions of generated SAWs were of interest and the directions were strongly related to the finger widths and spacings, the simplified model was sufficient for investigating the frequency-dependent feature of the CSFIT based acoustic tweezers. Input frequencies in the range of 13–18 MHz were used, matching the spacings of the IDTs. The two electrode groups in the modeled CSFIT were activated at harmonic voltage excitations to generate SAWs. To eliminate reflections from the edges of the model, perfectly matched layers (PML) and low-reflecting boundaries (LRBs) were added to the edges of the piezoelectric substrate, surrounding the area of interest (Fig. 2b). The shadowed region in Fig. 2c shows the terminals for applying excitation voltages.

Results

Directional SAWs generated by CSFITs

To investigate the generation of directional SAWs at different frequencies, finite element simulations using the model in Fig. 2b were performed. Fig. 2d shows the simulation result (field of displacement amplitude $|u_z|$) in the piezoelectric substrate. To characterize the generated SAWs at different excitation frequencies, the simulation results (field of displacement amplitude $|u_z|$) in the top surface of the piezoelectric substrate are plotted in Fig. 3a–d. These figures show that SAWs propagating in different directions are generated at four selected frequencies of 13.5, 14.4, 15.0, and 16.3 MHz. To quantitatively characterize the directionality of generated SAWs, the SAW amplitudes were extracted at the four frequencies and plotted in polar coordinate systems, as shown in Fig. 3e–h. The plots clearly show the angular variations of the generated SAW amplitudes. With an increase in the excitation frequency, the main lobe of the generated SAWs gradually rotated anticlockwise. Such anticlockwise changing of SAW directions is expected, since the spacing of the CSFIT decreases in this direction (yielding a higher resonance frequency). It can also be seen that as

the beam direction increases from Fig. 3e to 3h, the amplitudes of the SAWs increase. Such direction dependent effect on the SAW amplitudes could be induced by the anisotropic material properties of the $LiNbO_3$ substrate. The amplitude variations can affect the acoustic radiation forces applied on micro-objects in the SAW field. The amplitude variation can be compensated by controlling the excitation voltages at different frequencies.

The simulation results show that the CSFIT can generate SAWs in different directions by changing the excitation frequency. In addition to the SAW fields generated at the four frequencies in Fig. 3, other frequencies in the range from 13.5 to 16.3 MHz can be used to generate SAWs as well. To characterize the angular resolutions of the generated beams in Fig. 3e to 3h, the beam width θ_w is calculated by measuring the angular difference between two points (with the half peak amplitude) on the leading and trailing edges of the main lobe. The beam widths for plots in Fig. 3e to 3h are 31°, 34°, 41°, and 42°, respectively. To further reduce the beam width and improve the angular resolution, in the future, we will optimize the angular changing rate of the electrode spacing ($d\theta/\theta$) and the diameter of the CSFIT.

1D and 2D particle/cell patterning using CSFIT-based acoustic tweezers

With the fabricated CSFIT-based acoustic tweezers (Fig. 1b), we performed experiments to demonstrate the device's capability for patterning micro-objects into multiple configurations. Fig. 4 shows the result of 1D patterning, *i.e.*, distribution of K562 cells along parallel lines at four different frequencies. Movie S1† shows the dynamic process of aligning cells. From the experimental results, we see that cells are distributed in multiple 1D parallel lines with different skew angles and spatial periods. Moreover, the orientations of parallel patterns agree with the orientations of SAW fields predicted by simulations in Fig. 3. Although the simulated SAWs in Fig. 3a–d have curved wavefronts in the near-field region of the curved electrodes, the cell patterning results in Fig. 4 don't show any obvious curvatures. This is because the area for cell patterning in the microfluidic chamber is very small (nearly 4 wavelengths) and the location of the chamber is relatively far (nearly 15 wavelengths) from the electrodes.

The experimental results verify that our CSFIT-based acoustic tweezers can control the orientation and spacing of micro-objects patterns upon changing the excitation frequency. Moreover, the result in Fig. S3† shows that the cell viabilities are at relatively high levels (above 85%) within 15 min of exposure to the SAWs. With exposure duration increasing, the cell viability is slightly decreasing, probably due to the effect of acoustic radiation force.[51] In addition to the K562 cell, other types of cells (such as fibroblasts) can also be patterned by our acoustic tweezers. The current study focuses on the design of CSFITs and methodology. In the future, we will perform more tests on the effect of acoustic exposure on cells in addition to membrane integrity, and the potential implications of acoustic exposure on biological phenotype. The functionality of the 1D cell alignment can be used for investigating cell–cell interaction, as well as creating artificial tissues with different microscale structures.

The developed CSFIT-based acoustic tweezers generate 2D SSAWs by using excitation signals with two frequency components. As illustrated in Fig. S2,† when the excitation signals contain frequencies of [f_{θ_1}, f_{θ_2}], two pairs of CSFIT subsections along the directions

of θ_1 and θ_2 will excite SAWs. Through the interference of SAWs along the two directions, SSAWs will be generated with 2D periodic pressure nodes and antinodes. The pressure nodes are distributed in the form of a 2D grid-like array. We demonstrated 2D particle patterning using 10.2 μm yellow-green polystyrene (PS) particles. Because particles can be trapped by the pressure nodes, a 2D grid-like pattern of particles can be constructed. Those 2D patterns can also be considered as 2D lattices with rectangular or parallelogram-shaped unit cells. Some 2D configurations are shown in Fig. 5.

Dynamic reconfiguration of particle patterns

The fabricated CSFIT allows for tuning the generated SAWs by modulating the frequency and phase information in the excitation signal. Hence, the CSFIT-based acoustic tweezers can be used for controlling the SAW fields and dynamic reconfiguration of particle patterns. Here, we demonstrate two types of dynamic reconfigurations, including frequency-based pattern transformation and phase-based pattern translation. These two types of fundamental manipulations can be sequentially performed to achieve other complex manipulations.

For pattern transformation, the experimental results show when the excitation signal has two frequency components [15.70, 14.53] MHz, PS particles are trapped at pressure nodes and form the parallelogram-shaped 2D patterns shown in Fig. 5a. By changing the frequency combinations to [15.70, 17.04] MHz, the 2D pattern in Fig. 5a can be “twisted” to form another pattern with parallelogram-shaped unit cells as shown in Fig. 5b. The interior angles of the two types of lattices are 80° and 110°, respectively. Movie S2† shows the dynamic transformation process.

To realize pattern translation, we lock the frequency compositions and then gradually tune the phase difference between input signals for the two CSFITs. By tuning the phase difference, the positions of pressure nodes can be dynamically translated in-plane, enabling the synchronized translation of a particle pattern. Using the phase-based tuning method, we experimentally demonstrate that particle clusters in a 2D pattern in Fig. 5c can be translated to new positions shown in Fig. 5d. The phase-based translation process can be clearly seen in Movie S3.† In the video, the pattern moved 1/8 of a wavelength with every 45 degree phase increase.

Dynamic manipulation of single microparticles

In the experiments described above, we have shown that a 2D pattern can be translated in-plane with all the particle clusters moving simultaneously by tuning the phase difference. When only one particle is trapped in the pressure node, the single particle will be translated in-plane by tuning the phase difference. The relation between phase difference $\delta\boldsymbol{\varphi} = [\delta\boldsymbol{\varphi}_{\theta_1}, \delta\boldsymbol{\varphi}_{\theta_2}]$, and translation vector $\delta\boldsymbol{x}$ can be predicted by the following relationship,

$$\Delta\,\boldsymbol{x} = \frac{\lambda_{\theta_1}\,\delta\,\varphi_{\theta_1}}{4\,\pi}\mathbf{e}_{\theta_1} + \frac{\lambda_{\theta_2}\,\delta\,\varphi_{\theta_2}}{4\,\pi}\mathbf{e}_{\theta_2}, \tag{1}$$

where λ_{θ_1} and λ_{θ_2} are the wavelengths of the SAWs generated by angular subsections of CSFITs in directions of θ_1 and θ_2. $\mathbf{e}_{\theta_1}$ and $\mathbf{e}_{\theta_2}$ are unit vectors along the θ_1 and θ_2

directions. Note that in our experiment, we chose two directions with $\mathbf{e}_{\theta_1}$ and $\mathbf{e}_{\theta_2}$ being orthogonal.

Using the CSFIT-based acoustic tweezers, we are able to dynamically translate a single microparticle along different paths with high controllability. Dynamic translation can be performed through the following steps. First, two frequency components are identified following the preference that the unit direction vectors are orthogonal. Then, the desired translation path for the particle is spatially discretized into an array of N points at positions $[\boldsymbol{x}_i]_N$. Based on the positions and eqn (1), a series of required phase differences $[\delta\varphi_i]_N$ can be determined. Lastly, the phase differences are sequentially applied to the input signal for CSFITs through a function generator controlled with a MATLAB script. We experimentally demonstrate that a 10 μm PS particle can be moved following two different paths to write the letters “D” and “E”, as shown in Movie S4† and stacked optical images in Fig. 6a. We also investigated the speed and stability for moving 10 μm PS particles with our CSFIT-based acoustic tweezers. The result in Fig. 6b shows that the allowable velocity with an error less than 10% is nearly 15 μm s^{-1}; the phase change rate must be less than 45 degree s^{-1} for stable operation. Our experimental results show that the CSFIT-based acoustic tweezers can achieve precise dynamic manipulation of single microparticles simply by modulating the phase differences encoded in the excitation signals.

Conclusions

In this study, we present CSFIT based acoustic tweezers that can achieve dynamic and reconfigurable manipulations of microparticles and cells. CSFITs can tune the propagation direction of SAWs upon changing the excitation frequency, and they simultaneously generate/control SAWs in multiple directions by using a multi-tone input signal.

In a CSFIT, the finger widths and spacings gradually change along the angular direction of the transducer. Because of the angular spacing variation, different angular sections in the transducer respond to different excitation frequencies. Compared to traditional IDTs used for acoustofluidics,[45,52–55] the CSFIT offers two advantages: (i) continuous steering of the SAW propagation direction by tuning the excitation frequency; and (ii) simultaneous generation and independent control of SAWs in multiple directions using a multi-tone input signal.

With the new features offered by CSFITs, we can simply use an excitation signal with multiple frequency components (tones) to control multiple angular sections of the CSFITs. Hence, it becomes possible to use one signal to control SAWs in multiple directions without using complex electronics. For the CSFIT-based acoustic tweezers, we can simply modulate phase, amplitude, and frequency in multi-tone excitation signals to generate various potential well distributions for realizing different acoustofluidic functions. Through experiments, we demonstrated a range of functions by using a single device with one input channel, including multiconfiguration 1D and 2D patterning, dynamic reconfiguration of 2D patterns, and dynamic manipulation of single microparticles. In our experiments, multi-tone excitation signals with two frequencies are used for generating 2D grid-like patterns and translation of particles. In the future, we will optimize the design of CSFITs and use them to generate more complex patterns with more frequencies.

Our work offers a new way to control SAWs for acoustofluidic applications. The CSFIT enables simultaneous generation and independent control of SAWs in different directions with low requirements of electronic hardware such as multichannel function generators, multiplexers, and multiple amplifiers. The CSFIT based acoustic tweezers presented in this work have the potential to inspire the design of other acoustic tweezers for lab-on-a-chip applications such as the sorting, printing, patterning, and separation of cells.

Supplementary Material

Refer to Web version on PubMed Central for supplementary material.

Acknowledgements

We acknowledge support from the National Institutes of Health (R01GM132603, UG3TR002978, R01HD086325, R44GM125439, R33CA223908, R43HL140800, and R01GM127714) and United States Army Medical Research Acquisition Activity (W81XWH-18-1-0242). Haodong Zhu, Shuaiguo Zhao and Zeyu Wang acknowledge financial support from the China Scholarship Council.

References

1. Ozcelik A, Rufo J, Guo F, Gu Y, Li P, Lata J and Huang TJ, Nat. Methods, 2018, 15, 1021–1028. [PubMed: 30478321]
2. Walker GM, Zeringue HC and Beebe DJ, Lab Chip, 2004, 4, 91–97. [PubMed: 15052346]
3. Menciassi A, Eisinberg A, Izzo I and Dario P, IEEE ASME Trans. Mechatron, 2004, 9, 311–320.
4. Chiou PY, Ohta AT and Wu MC, Nature, 2005, 436, 370. [PubMed: 16034413]
5. Voldman J, Annu. Rev. Biomed. Eng, 2006, 8, 425–454. [PubMed: 16834563]
6. Nilsson J, Evander M, Hammarström B and Laurell T, Anal. Chim. Acta, 2009, 649, 141–157. [PubMed: 19699390]
7. Villone MM, Memmolo P, Merola F, Mugnano M, Miccio L, Maffettone PL and Ferraro P, Lab Chip, 2018, 18, 126–131.
8. Lam KH, Li Y, Li Y, Lim HG, Zhou Q and Shung KK, Sci. Rep, 2016, 6, 37554. [PubMed: 27874052]
9. Ashkin A, Dziedzic JM, Bjorkholm J and Chu S, Opt. Lett, 1986, 11, 288–290. [PubMed: 19730608]
10. Zhang H and Liu K-K, J. R. Soc., Interface, 2008, 5, 671–690. [PubMed: 18381254]
11. Probst R and Shapiro B, J. Micromech. Microeng, 2011, 21, 027004.
12. Bausch AR, Möller W and Sackmann E, Biophys. J, 1999, 76, 573–579. [PubMed: 9876170]
13. De Vlaminck I and Dekker C, Annu. Rev. Biophys, 2012, 41, 453–472. [PubMed: 22443989]
14. Shi J, Ahmed D, Mao X, Lin S-CS, Lawit A and Huang TJ, Lab Chip, 2009, 9, 2890–2895. [PubMed: 19789740]
15. Ding X, Lin S-CS, Kiraly B, Yue H, Li S, Chiang I-K, Shi J, Benkovic SJ and Huang TJ, Proc. Natl. Acad. Sci. U. S. A, 2012, 109, 11105–11109. [PubMed: 22733731]
16. Wiklund M, Green R and Ohlin M, Lab Chip, 2012, 12, 2438–2451. [PubMed: 22688253]
17. Zhang SP, Lata J, Chen C, Mai J, Guo F, Tian Z, Ren L, Mao Z, Huang P-H and Li P, Nat. Commun, 2018, 9, 2928. [PubMed: 30050088]
18. Zhao S, He W, Ma Z, Liu P, Huang P-H, Bachman H, Wang L, Yang S, Tian Z and Wang Z, Lab Chip, 2019, 19, 941–947. [PubMed: 30702741]
19. Shaglwf Z, Hammarström B, Shona Laila D, Hill M and Glynne-Jones P, J. Acoust. Soc. Am, 2019, 145, 945–955. [PubMed: 30823821]
20. Melde K, Choi E, Wu Z, Palagi S, Qiu T and Fischer P, Adv. Mater, 2018, 30, 1704507.
21. Meng L, Cai F, Li F, Zhou W, Niu L and Zheng H, J. Phys. D: Appl. Phys, 2019, 52, 273001.

22. Baudoin M and Thomas J-L, Annu. Rev. Fluid Mech, 2020, 52, 205–234.
23. Bruus H, Lab Chip, 2012, 12, 1014–1021. [PubMed: 22349937]
24. Gedge M and Hill M, Lab Chip, 2012, 12, 2998–3007. [PubMed: 22842855]
25. Mao Z, Li P, Wu M, Bachman H, Mesyngier N, Guo X, Liu S, Costanzo F and Huang TJ, ACS Nano, 2017, 11, 603–612. [PubMed: 28068078]
26. Tian Z, Yang S, Huang P-H, Wang Z, Zhang P, Gu Y, Bachman H, Chen C, Wu M and Xie Y, Sci. Adv, 2019, 5, eaau6062. [PubMed: 31172021]
27. Cacace T, Memmolo P, Villone MM, De Corato M, Mugnano M, Paturzo M, Ferraro P and Maffettone PL, Lab Chip, 2019, 19, 3123–3132. [PubMed: 31429851]
28. Guo F, Mao Z, Chen Y, Xie Z, Lata JP, Li P, Ren L, Liu J, Yang J and Dao M, Proc. Natl. Acad. Sci. U. S. A, 2016, 113, 1522–1527. [PubMed: 26811444]
29. Wu M, Ozcelik A, Rufo J, Wang Z, Fang R and Huang TJ, Microsyst. Nanoeng, 2019, 5, 32. [PubMed: 31231539]
30. Petersson F, Åberg L, Swärd-Nilsson A-M and Laurell T, Anal. Chem, 2007, 79, 5117–5123. [PubMed: 17569501]
31. Wu M, Ouyang Y, Wang Z, Zhang R, Huang P-H, Chen C, Li H, Li P, Quinn D and Dao M, Proc. Natl. Acad. Sci. U. S. A, 2017, 114, 10584–10589. [PubMed: 28923936]
32. Li P and Huang TJ, Anal. Chem, 2019, 91, 757–767. [PubMed: 30561981]
33. Xie Y, Bachman H and Huang TJ, TrAC, Trends Anal. Chem, 2019, 117, 280–290.
34. Ren L, Yang S, Zhang P, Qu Z, Mao Z, Huang PH, Chen Y, Wu M, Wang L and Li PJS, Small, 2018, 14, 1801996.
35. Franke T, Braunmüller S, Schmid L, Wixforth A and Weitz D, Lab Chip, 2010, 10, 789–794. [PubMed: 20221569]
36. Nama N, Huang P-H, Huang TJ and Costanzo F, Biomicrofluidics, 2016, 10, 024124. [PubMed: 27158292]
37. Ahmed H, Park J, Destgeer G, Afzal M and Sung HJ, Appl. Phys. Lett, 2019, 114, 043702.
38. Reboud J, Bourquin Y, Wilson R, Pall GS, Jiwaji M, Pitt AR, Graham A, Waters AP and Cooper JM, Proc. Natl. Acad. Sci. U. S. A, 2012, 109, 15162–15167. [PubMed: 22949692]
39. Wu C, Lillehoj PB, Sabet L, Wang P and Ho CM, Biotechnol. J, 2011, 6, 150–155. [PubMed: 21259440]
40. Guo F, Zhou W, Li P, Mao Z, Yennawar NH, French JB and Huang TJ, Small, 2015, 11, 2733–2737. [PubMed: 25641793]
41. Collins DJ, Morahan B, Garcia-Bustos J, Doerig C, Plebanski M and Neild A, Nat. Commun, 2015, 6, 8686. [PubMed: 26522429]
42. Silva GT, Lopes JH, Leão-Neto JP, Nichols MK and Drinkwater BW, Phys. Rev. Appl, 2019, 11, 054044.
43. Collins DJ, O'Rorke R, Devendran C, Ma Z, Han J, Neild A and Ai Y, Phys. Rev. Lett, 2018, 120, 074502. [PubMed: 29542954]
44. Zhang L, J. Acoust. Soc. Am, 2018, 144, 443–447. [PubMed: 30075669]
45. Shilton R, Tan MK, Yeo LY and Friend JR, J. Appl. Phys, 2008, 104, 014910.
46. Riaud A, Baudoin M, Matar OB, Becerra L and Thomas J-L, Phys. Rev. Appl, 2017, 7, 024007.
47. Riaud A, Baudoin M, Thomas J-L and Matar OB, IEEE Trans. Ultrason. Ferroelectr. Freq. Control, 2016, 63, 1601–1607. [PubMed: 28873055]
48. Ding X, Shi J, Lin S-CS, Yazdi S, Kiraly B and Huang TJ, Lab Chip, 2012, 12, 2491–2497. [PubMed: 22648600]
49. Wu T-T and Chang I-H, J. Appl. Phys, 2005, 98, 024903.
50. Zhang J, Yang S, Chen C, Hartman JH, Huang P-H, Wang L, Tian Z, Zhang P, Faulkenberry D, Meyer JN and Huang TJ, Lab Chip, 2019, 19, 984–992. [PubMed: 30768117]
51. Wiklund M, Lab Chip, 2012, 12, 2018–2028. [PubMed: 22562376]
52. Asai K, Kurosawa MK and Higuchi T, Electron. Commun. Jpn, 2004, 87, 10–19.
53. Wu T-T, Tang H-T, Chen Y-Y and Liu P-L, IEEE Trans. Ultrason. Ferroelectr. Freq. Control, 2005, 52, 1384–1392. [PubMed: 16245608]

54. Laude V, Gérard D, Khelfaoui N, Jerez-Hanckes CF, Benchabane S and Khelif A, Appl. Phys. Lett, 2008, 92, 094104.

55. Friend J and Yeo LY, Rev. Mod. Phys, 2011, 83, 647.

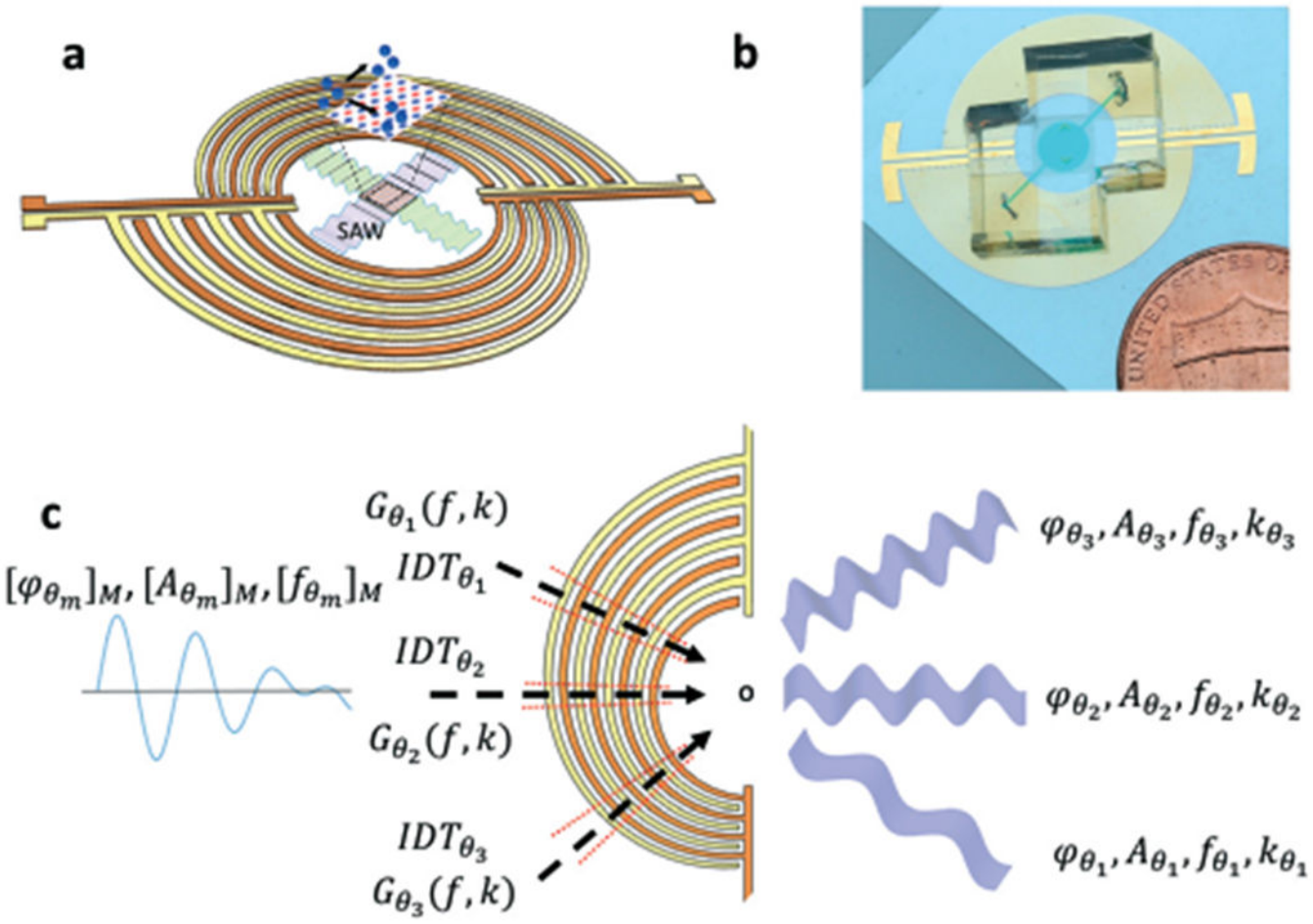

Fig. 1.

Mechanism of CSFIT-based acoustic tweezers. (a) Device schematic and (b) photograph of the device with a disposable microfluidic chamber. (c) The principle of controlling CSFITs with a multi-tone excitation signal. The multi-tone signal with phases $[\varphi_{\theta_m}]_M$ and amplitude $[A_{\theta_m}]_M$ at frequencies $[f_{\theta_m}]_M$ is decomposed by the CSFIT for generating three travelling SAWs in different directions.

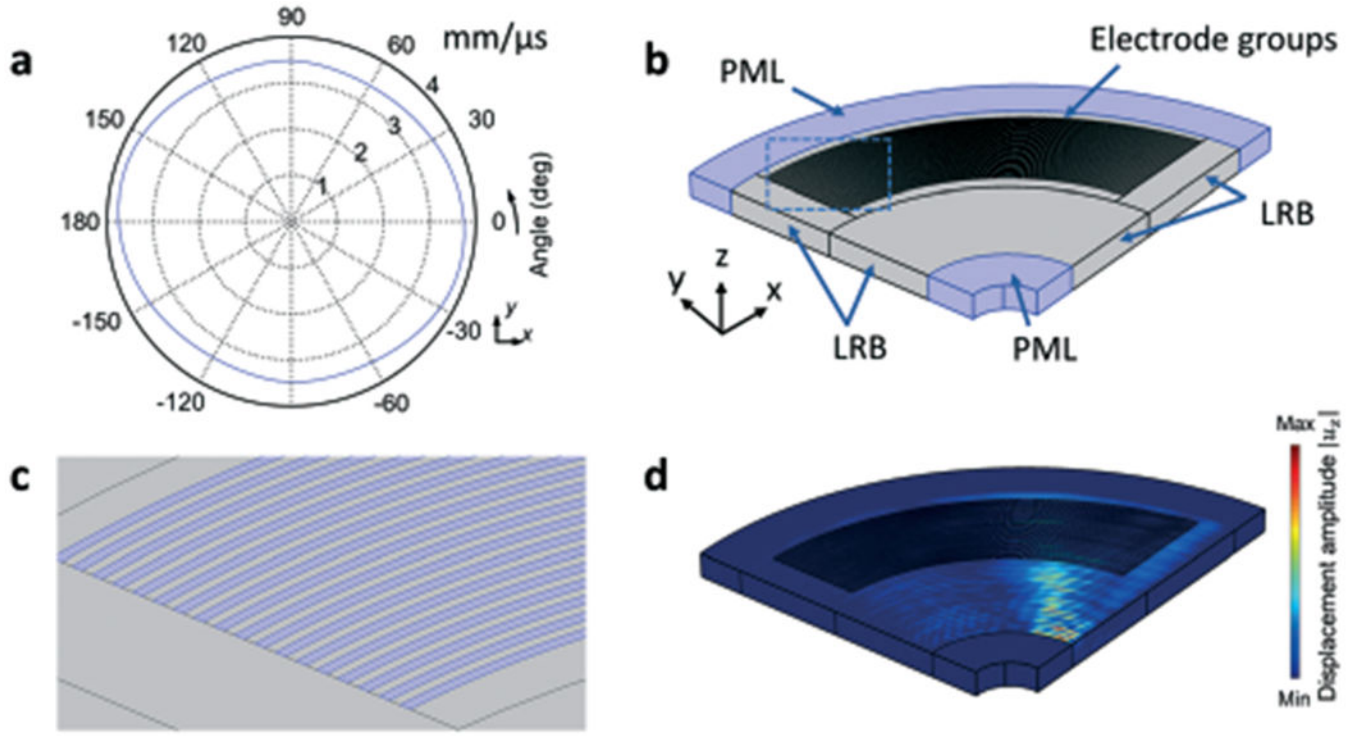

Fig. 2.

The finite element model used to simulate CSFIT. (a) Direction-dependent phase velocity c_θ of SAWs in the X-cut $LiNbO_3$ substrate. (b) Schematic of the simulation setup. The finite element model is composed of a 0.8 mm-thick X-cut $LiNbO_3$ substrate with a CSFIT that has two groups of electrodes. (c) Zoom-in view of electrodes. (d) 3D simulation of the displacement field u_z for the travelling SAW generated at the excitation frequency of 13.5 MHz.

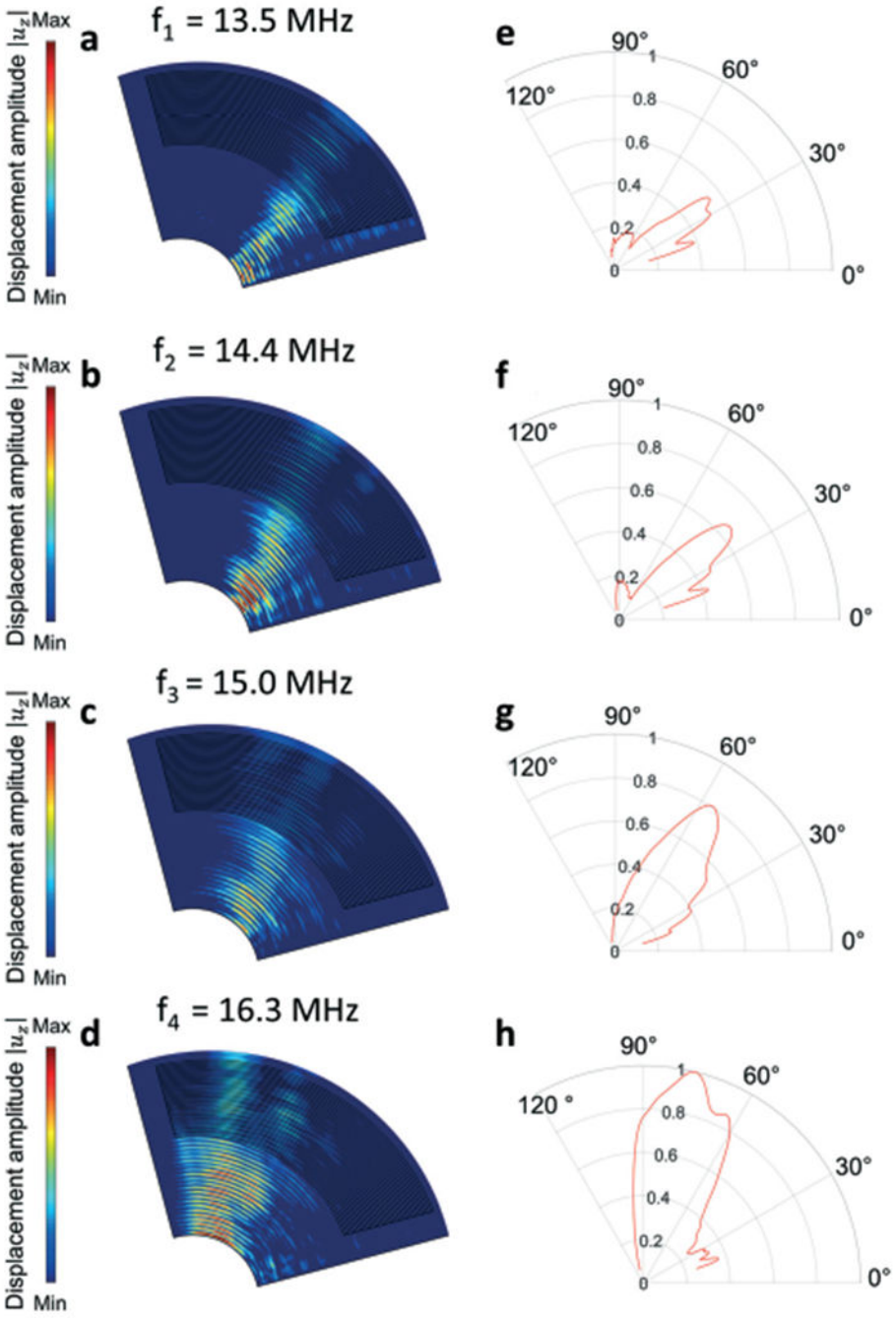

Fig. 3.

Simulation results at different excitation frequencies. (a–d) Fields of SAW displacement amplitudes $|u_z|$ on the top surface of the piezoelectric substrate. The four fields are simulated at four excitation frequencies of 13.5, 14.4, 15.0, and 16.3 MHz, respectively. (e–h) Angular variations of normalized SAW amplitudes in the polar coordinate system at the four frequencies.

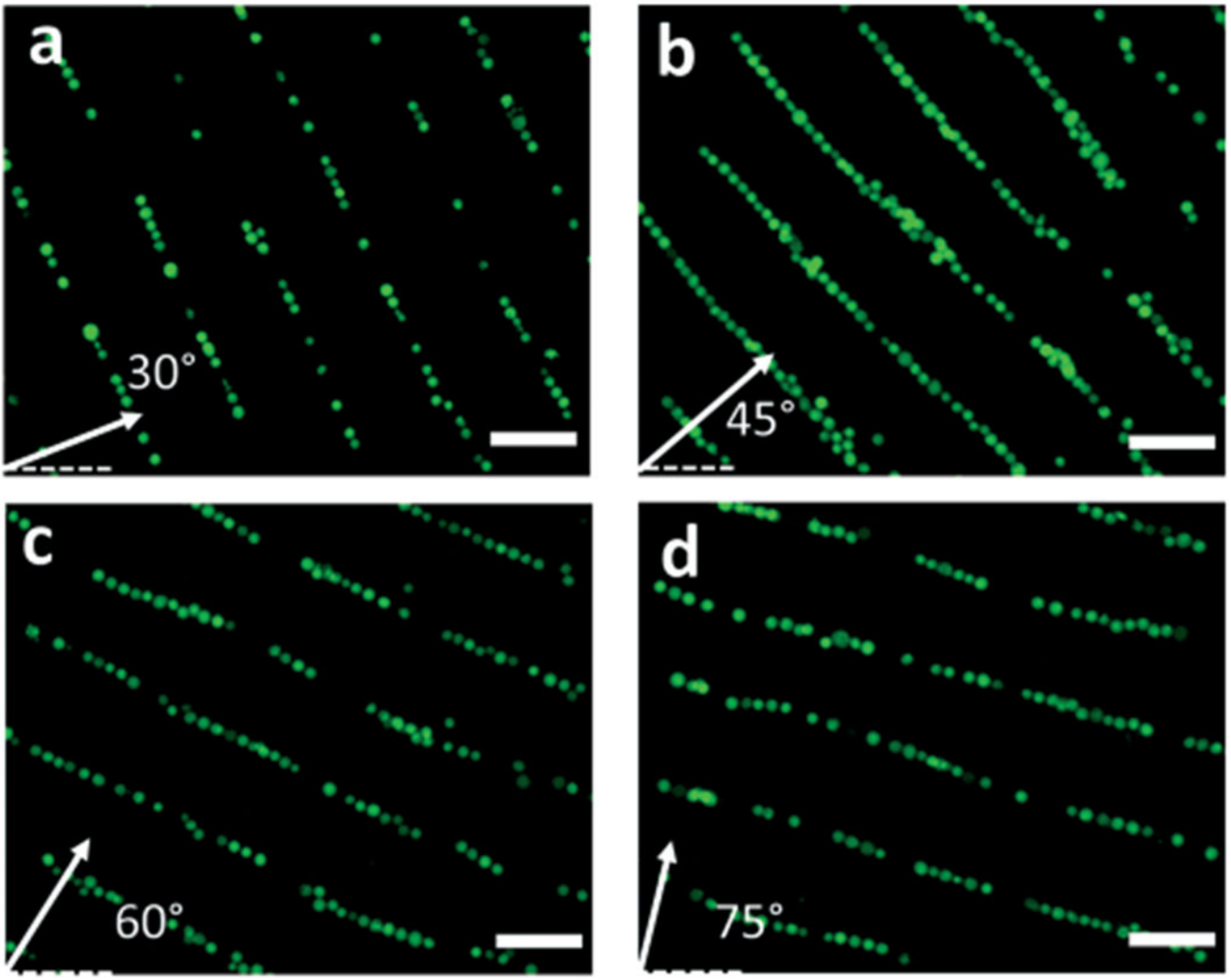

Fig. 4.

Multi-configuration 1D patterning of K562 cells using CSFIT-based acoustic tweezers. (a–d) Microscopy images of K562 cells taken by a CCD camera at the four excitation frequencies. Micro-objects are distributed in multiple 1D, parallel line-like patterns with different skew angles and interspacing. The pattern orientations agree with the orientations of SAW wave fronts in the simulation results (Fig. 3).

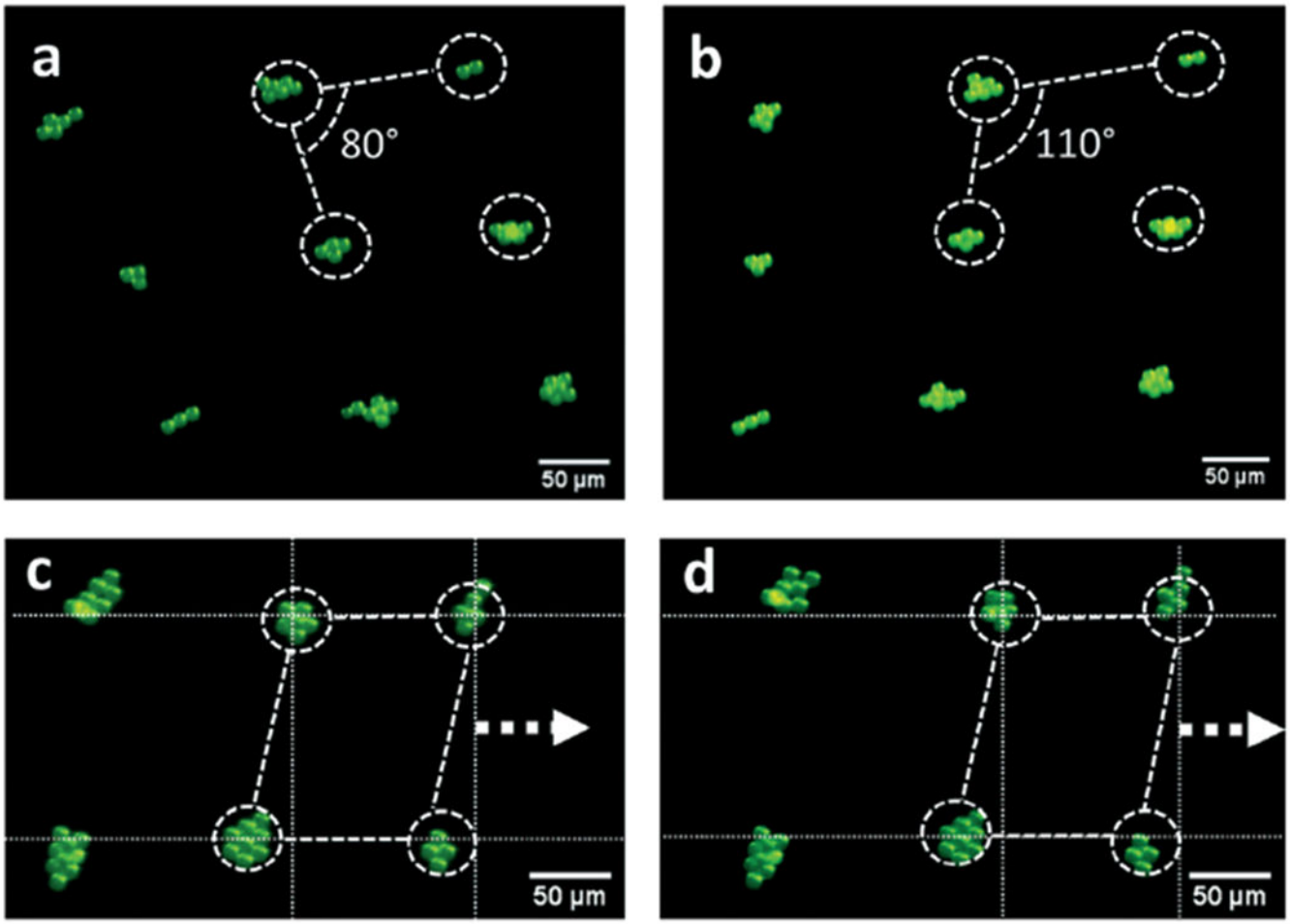

Fig. 5.

Multi-configuration 2D patterning configuration and pattern reconfiguration of PS particles. By switching the excitation frequency combinations, the particle pattern in (a) can be transformed to the pattern in (b). By tuning the phase information of the multi-tone excitation signal, the 2D pattern in (c) can be translated in-plane and become the distribution in (d).

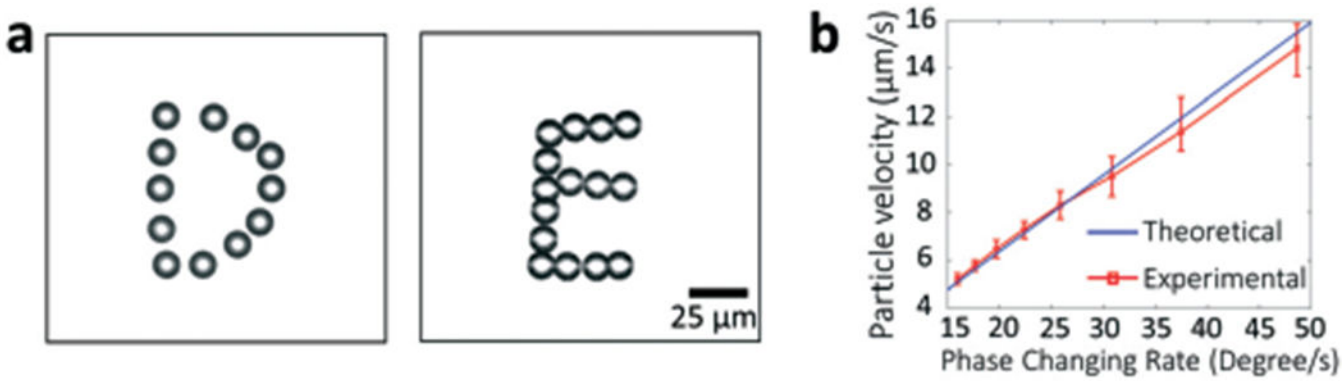

Fig. 6.

Dynamic manipulation of a 10 μm PS particle using CSFIT-based acoustic tweezers. (a) Stacked optical images acquired during the acoustic manipulation. The images show two characters, “D” and “E”. (b) Characterization of the particle velocity at different phase changing rates.